

**INTERNATIONAL JOURNAL OF HEAT AND MASS TRANSFER**

*EDITOR: Professor R. Grief, Mechanical Engineering Department, University of California at Berkeley,  
Berkeley, California, USA.*

**ACCEPTED MARCH 25<sup>TH</sup> 2017**

**IMPACT FACTOR= 2.857**

**ELECTROTHERMAL TRANSPORT OF NANOFUIDS VIA PERISTALTIC PUMPING IN A FINITE  
MICRO-CHANNEL: EFFECTS OF JOULE HEATING AND HELMHOLTZ-SMOLUCHOWSKI VELOCITY**

**<sup>^1</sup>Dharmendra Tripathi, <sup>1</sup>Ashish Sharma and <sup>2</sup>O. Anwar Bég**

*<sup>1</sup>Department of Mechanical Engineering, Manipal University, Jaipur-303007, India.*

*<sup>2</sup> Fluid Dynamics, Bio-Propulsion and Nanosystems, Department of Mechanical and Aeronautical Engineering, Salford University, Newton Building, The Crescent, Salford, M54WT, England, UK.*

**<sup>^</sup>Corresponding author: D. Tripathi (dharmtri@gmail.com)**

**ABSTRACT**

The present article studies theoretically the electrokinetic pumping of nanofluids with heat and mass transfer in a micro-channel under peristaltic waves, a topic of some interest in medical nano-scale electro-osmotic devices. The microchannel walls are deformable and transmit periodic waves. The Chakraborty-Roy nanofluid electrokinetic formulation is adopted in which Joule heating effects are incorporated. Soret and Dufour cross-diffusion effects are also considered. Under low Reynolds number (negligible inertial effects), long wavelength and Debye linearization approximations, the governing partial differential equations for mass, momentum, energy and solute concentration conservation are derived with appropriate boundary conditions at the micro-channel walls. The merging model features a number of important thermo-physical, electrical and nanoscale parameter, namely thermal and solutal Grashof numbers, the Helmholtz-Smoluchowski velocity (maximum electro-osmotic velocity) and Joule heating to surface heat flux ratio. Closed-form solutions are derived for the solute concentration, temperature, axial velocity, averaged volumetric flow rate, pressure difference across one wavelength, and stream function distribution in the wave frame. Additionally expressions are presented for the surface shear stress function at the wall (skin friction coefficient), wall heat transfer rate (Nusselt number) and wall solute mass transfer rate (Sherwood number). The influence of selected parameters on these flow variables is studied with the aid of graphs. Bolus formation is also visualized and analyzed in detail.

**Keywords:** *Electrokinetic nanofluids; heat and mass transfer; peristalsis; Joule heating; nanoscale pumps.*

**1. INTRODUCTION**

Nanoscale engineering has emerged as a substantial development in the 21<sup>st</sup> century. Such systems can achieve performance that is not possible at the macroscale. Nanotechnology includes nanomaterial developments and an important sub-category in

this regard is *nanofluids*. Introduced by Choi [1] these fluids achieve higher thermal conductivities and convective heat transfer coefficients as compared with conventional base fluids (e.g. air and water). Nanofluids are synthesized by suspending nanoparticles which may be metallic/non-metallic and are generically 1-100 nanometers in dimension, in base fluids and have been deployed in an extensive range of technologies many of which have been reviewed lucidly by Taylor *et al.* [2]. These include lubrication systems where heat can be dissipated more effectively with nanofluids [3], heat exchangers in solar power plants [4], anti-bacterial agents in biotechnological sterilization [5], nano-bioconvection microbial fuel cells (MFCs) using combined silver nanoparticles and gyrotactic micro-organisms [6], hyperthermia medications [7] and nano-coated drug delivery systems [8]. Although for the first decade most research in nanofluids was focused on laboratory and property-based experimentation, in recent years mathematical modelling has emerged as an important new area. Numerous geometrical systems have been explored and both steady and unsteady flows analyzed. Yadav *et al.* [9] investigated the Rayleigh-Benard problem for nanofluids, using a linear hydrodynamic stability approach. Basir *et al.* [10] examined the enrobing hydrodynamics, heat and mass transfer in transient axisymmetric boundary layer flow of bioconvective nanofluids from an extending cylindrical body using Maple software. Zaimi *et al.* [11] used a homotopy method to study the stagnation flow of nanofluids with bioconvection from a contracting or extending two-dimensional sheet. These studies all confirmed the marked influence of nano-particles on Nusselt and Sherwood numbers.

In parallel with the above developments, modern microfluidic systems are also being continuously investigated. In such systems electro-kinetics (or electro-osmosis) plays a significant role. Although first identified over two centuries ago by Reuss [12], electro-osmosis has more recently infiltrated into many sophisticated microscale designs including bio-chip systems for drug delivery, biomedical diagnostics and bio-micro-electro-mechanical-systems (bioMEMS). Electrokinetics involves the dynamics of electrolytes (ionic solutions) and is generated by the imposition of an external electric field in an electrolyte-filled conduit with electric double layers on its wetted surfaces. The microscopic (or smaller) scale of bioMEMS amplifies the effect of the Coulomb electrical forces and this in turn greatly modifies micro-channel transport processes. The

multi-physical nature of electrokinetic phenomena also makes this area particularly attractive to interdisciplinary engineering sciences since mathematical models must describe accurately the interplay between electrical, viscous and other body forces (buoyancy, magnetic, rotational) and complex geometric features. Electro-osmotic flow provides enhanced flow control at lower volumetric flow rates compared with conventional pressure-driven flows. Interesting developments in electrokinetic engineering sciences include separation of emulsions in microchannel-membrane systems, valve designs for pharmacological delivery [13] in which the flow rate is regulated by electrical current passing through the membrane, skin iontophoresis systems [14], soap film manipulation [15] with electrohydrodynamic induction and electro-kinetic DNA concentrators [16]. Mathematical studies of electrokinetic transport have featured many analytical and also numerical methods. Dejam *et al.* [17] studied analytically the shear dispersion a neutral non-reacting chemical species within a channel with porous walls, under the dual effects of pressure-driven and electro-osmotic flow, and computed the dispersion coefficient as a function of the Debye–Hückel parameter, Poiseuille contribution fraction, and Péclet number. Moreau *et al.* [18] explored both computationally and experimentally the use of electro-osmosis in removing contaminants in geomaterials. Jian *et al.* [19] employed a Laplace transform method to derive closed-form solutions for time-dependent electro-kinetic viscoelastic flow in a micro-channel, describing the influence of viscosity ratio, density ratio, dielectric constant ratio, relaxation time, interface charge density jump, and interface zeta potential difference on velocity evolution. Liang *et al.* [20] used a computational flow code to investigate the electro-osmotic flow (EOF) perturbations generated close to a membrane surface within an unobstructed empty membrane channel aimed at elevating wall shear and thereby delaying the onset of fouling for nanofiltration and reverse osmosis processes. Iverson *et al.* [21] studied analytically the influence of duct aspect ratio and volumetric heat generation and Peclet number on heat transfer in electro-osmotic rectangular ducts with isothermal boundary conditions and vanishing Debye layer thickness. They showed that fully developed Nusselt number is reduced from a maximum for the parallel plate configuration to a minimum for the square duct scenario and furthermore that electro-kinetically generated flow achieves significantly longer thermal entry zones compared

with pressure-driven flow. A similar study has been communicated by Broderick *et al.* [22] but for larger values of electrical double layer thickness. Schit *et al.* [23] considered the electro-osmotic flow and heat transfer of power-law bio-fluids in a micro-channel with Joule electro-thermal heating effects, with thermal radiation and velocity slip condition. They considered the scenario wherein the channel depth is substantially greater than the thickness of electrical double layer comprising both the Stern and diffuse layers, and showed that increasing Joule heating parameter depresses Nusselt number for both pseudo-plastic and dilatant fluids.

An important possible development in micro-systems is the combination of nanofluids and electro-osmotic flow. The important potential significance of such systems i.e. nano-electro-kinetic devices has been described by Murshed *et al.* [24]. Dutta [25] has investigated the nanofluidic separation of non-neutral analytes using a pressure-gradient in combination with a counteracting electroosmotic flow field. Safarna *et al.* [26] studied the influence of an external electrical field on iron-oxide-water nanofluid flow and heat transfer in micro-channels using the finite volume method and the Maxwell-Garnetts (MG) and Brinkman models for thermal conductivity and viscosity. They found that Nusselt number is strongly influenced by Reynolds number and applied voltage. Choi *et al.* [27] examined the electrokinetic flow of charged nanoparticles in microfluidic aqueous NaCl solution Couette flow, noting for the first time, a strong deviation of the velocity profile from the classical linear Couette flow case. Rokni *et al.* [28] used numerical shooting quadrature to study electro-kinetic and magnetohydrodynamic body force effects on rotating nanofluid flows. They found that there is a strong elevation in Nusselt number with magnetic and electrical field parameters and also Reynolds number and a substantial depression with increasing rotation effect.

Peristaltic pumping is a biological process which efficiently transfers fluids via flexible conduits under progressive waves of contraction or expansion from a zone of lower pressure to higher pressure [29, 30]. Peristalsis in living organisms is an involuntary mechanism and features in numerous aspects of physiology including intestinal dynamics, swallowing, blood flow, embryology etc. However in biomimetic engineered designs, actuators can be deployed to achieve this transport. When combined with electro-osmotics and/or magnetohydrodynamics, very elegant and versatile microscale

and nanoscale pumps can be designed, as elucidated by Chang and Yossifon [31], Takamura *et al.* [32] and Reichmuth *et al.* [33]. These designs maximize the use of external electrical fields for microfluidic manipulation and enhanced directional control and also capitalize on valveless miniaturized configurations for eliminating tribological wear and leakage. Modern progress in hyperthermia, cryosurgery and laser diagnosis systems have also made heat transfer in electro-osmotic peristaltic pumps of great interest to engineers. Many sophisticated systems in this regard have been manufactured and tested in medicine and excellent works reporting such developments include Berg *et al.* [34] (two-stage peristaltic micropumps). Analysis of such systems was conducted for thermo-magnetic peristaltic pumps by Tripathi and Bég [35]. Other significant investigations include Mao *et al.* [36] who reported on the synthesis of a dielectric elastomeric peristaltic micro-pump and Loumes [37] who reported in a novel peristaltic multi-stage impedance pump utilizing a periodic asymmetrical compression on a segment of the transport vessel (elastic tube). Studies of peristaltic nanofluid pumping have also emerged in recent years, inspired by breakthroughs in nanoscale fabrication techniques and the desire to enhance thermal as well as hydrodynamic performance. Hayat *et al.* [38] considered double-diffusive peristaltic convection in tubes with wall slip and magnetic Joule effects. Abbasi *et al.* [39] studied rheological nanofluid pumping via peristalsis. Bég and Tripathi [40] considered dual thermal and species buoyancy effects in axisymmetric peristaltic nanofluid transport. Prasad *et al.* [41] derived analytical solutions for velocity profile, pressure drop, time averaged flux and frictional force in peristaltic flow through inclined tubes, for a range of wave forms, observing that a much larger bolus (trapped fluid zone) is achieved for single sinusoidal waves as compared with multi sinusoidal waves. Further studies of peristaltic nanofluid dynamics include Dhanapal *et al.* [42] who also studied rotational effects and Abbasi *et al.* [43] who analysed peristaltic flows of water-based silver nanoparticles in a symmetric channel with convective boundary conditions, heat generation and viscous dissipation effects, observing increased wall heat transfer rates are achieved with higher nanoparticle volume fraction is also reported. Interesting outcomes of this study are summarized. Electro-osmotic peristaltic flows of Newtonian fluids have also been studied. Chakraborty [44] considered the influence of axial electric field on microfluidic transport in peristaltic

microtubes, showing that careful prescription of peristalsis wave characteristics and axial electrokinetic body force may successfully boost the time-averaged flow rate in such systems. Tripathi *et al.* [45] derived analytical solutions for unsteady electro-osmotic peristaltic transport in a microchannel subjected to transverse magnetic field and axial electrical field, using lubrication and Debye approximations. They showed that stronger magnetic field discourages bolus and decelerates axial flow and flow rate but elevates pressure difference at low time values. They also found that lower Debye electrical length increases time-averaged flow rate but decelerates axial flow. Bandopadhyay *et al.* [46] have also presented a very recent analysis of electrokinetic peristaltic transport in microfluidic channels, considering different channel materials (polyvinyl chloride and Teflon) and presented closed-form expressions for the pressure drop and volumetric flow rate and demonstrating the improved electro-osmotic performance with simultaneous peristalsis and axial electric fields for aqueous solutions.

To the authors' knowledge the *combined electro-osmotic peristaltic flow of nanofluids* however, have received very little attention, despite many substantial applications in nanofluidic and microfluidic pumps. In the present investigation we study analytically the *influence of Joule electro-thermal heating on unsteady electrokinetic peristaltic transport of nanofluids in a micro-channel*. Soret and Dufour cross-diffusion effects are also considered and both thermal and species buoyancy effects included. Joule heating effects which arise due to the presence of electrical potential gradient and electrical current, have been considered earlier by Bosse *et al.* [47] and Petersen *et al.* [48] for Newtonian fluids and Sadeghi *et al.* [49] for non-Newtonian fluids. These studies have shown that Nusselt number at the micro-channel walls is strongly modified by Joule heating. The present study is motivated by exploring the modification (and thermal improvement) of micro/nanoscale devices in which electro-osmotic flows are used via both utilisation of peristaltic wave motion of the transmitting walls and also deployment of nanofluids as the working electrolyte medium. The work is therefore an extension of the earlier investigation by Chakraborty and Roy [50] which considered rigid walls. Analytical solutions to the non-dimensional, linearized boundary value problem are derived. The influence of Joule heating to wall heat flux ratio and Helmholtz-Smoluchowski velocity

(maximum electro-osmotic velocity) on fluid, heat and mass transfer characteristics are presented graphically and interpreted at length.

## 2. MATHEMATICAL FORMULATION AND ANALYTICAL SOLUTIONS

The geometric of an electro-osmotic nanofluid peristaltic micro-channel is depicted in **Fig.1**. The geometric relation for the peristaltic waves imposed on the micro-channel walls is as follows:

$$\bar{h}(\bar{x}, \bar{t}) = a - \bar{\phi} \cos^2 \frac{\pi}{\lambda} (\bar{x} - c\bar{t}), \quad (1)$$

where  $\bar{h}, \bar{x}, \bar{t}, a, \bar{\phi}, \lambda$  and  $c$  denote the transverse displacement of the walls, axial coordinate, time, half width of the channel, amplitude of the wave, wavelength and wave velocity respectively. The temperature and solute concentration at the center line and the walls of the microfluidics channel are given as:  $\bar{T} = T_0, \bar{C} = C_0$ , (at  $\bar{y} = 0$ ),  $\bar{T} = T_1, \bar{C} = C_1$ , (at  $\bar{y} = \bar{h}$ ).

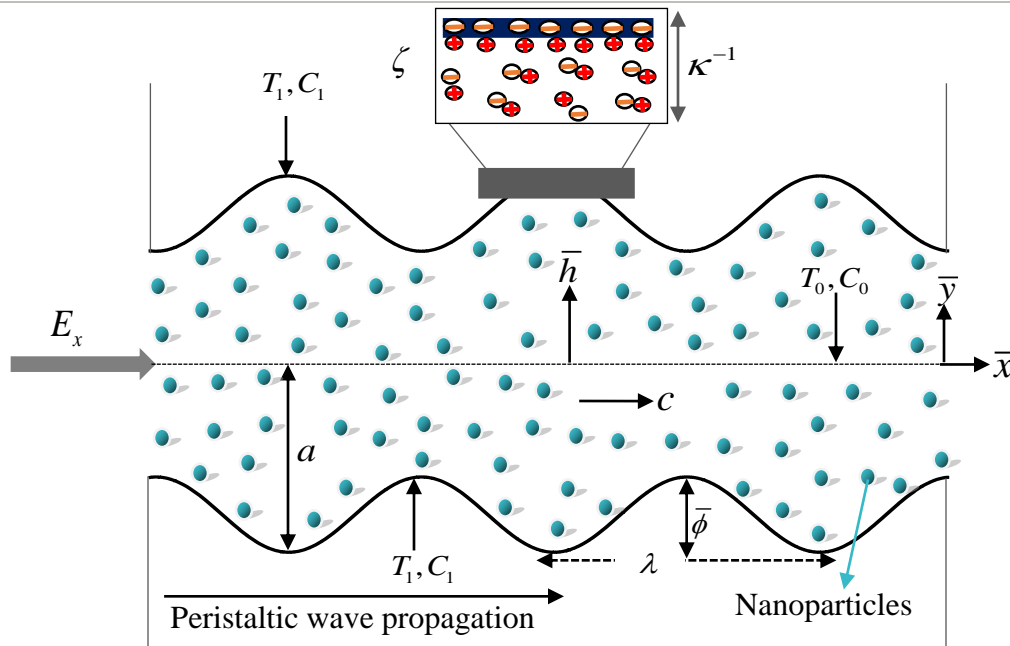


**Figure 1.** Schematic diagram of electroosmosis–modulated peristaltic transport of nanofluids through the microfluidics channels subjected to constant temperature and solute concentration ( $\bar{T} = T_1, \bar{C} = C_1$ ) at the top and bottom channel walls and  $\bar{T} = T_0, \bar{C} = C_0$  at center of channel. An external electric field ( $E_x$ ) is applied to alter the flow.

We consider the viscous, incompressible, time-dependent, electro-osmosis-modulated peristaltic transport of nanofluids through a finite micro-channel. To mathematically model the physical problem, the continuity, momentum, energy and solute concentration equations are formulated in vector notation as:

$$\nabla \cdot \mathbf{q} = 0, \quad (2)$$

$$\rho_{ef} \left( \frac{\partial \mathbf{q}}{\partial t} + (\mathbf{q} \cdot \nabla) \mathbf{q} \right) = -\nabla \bar{p} + \mu_{ef} \nabla^2 \mathbf{q} + \mathbf{f}_g + \bar{\rho}_e E_x, \quad (3)$$

$$(\rho c_p)_{ef} \left( \frac{\partial \bar{T}}{\partial t} + (\mathbf{q} \cdot \nabla) \bar{T} \right) = k_{ef} \nabla^2 \bar{T} + D_{tc} \nabla^2 \bar{C} + \mu_{ef} \varphi + \sigma_{ef} E_x^2, \quad (4)$$

$$\frac{\partial \bar{C}}{\partial t} + (\mathbf{q} \cdot \nabla) \bar{C} = D_s \nabla^2 \bar{C} + D_{ct} \nabla^2 \bar{T}, \quad (5)$$

where,  $\mathbf{q} \equiv (\bar{u}, \bar{v})$  is velocity vector,  $\nabla \equiv i \frac{\partial}{\partial x} + j \frac{\partial}{\partial y}$  and  $\nabla^2 = \nabla \cdot \nabla \equiv \frac{\partial^2}{\partial x^2} + \frac{\partial^2}{\partial y^2}$  are

Hamilton operator and Laplace operator respectively,  $\mathbf{f}_g = \rho_{ef} g \{ \beta_t (\bar{T} - T_0) + \beta_c (\bar{C} - C_0) \}$ .

And  $\rho, \bar{p}, \mu, \bar{\rho}_e, E_x, c_p, \bar{T}, \bar{C}, k, \sigma, \varphi, D_s, D_{tc}, D_{ct}$  are the density, pressure, viscosity, electrical charge density, applied electrical field, specific heat at constant pressure, temperature, solute concentration, thermal conductivity, electrical conductivity, viscous dissipation function, solutal diffusivity of the electrolyte Dufour diffusivity and Soret diffusivity where the subscript ( $ef$ ) refers to the effective property nanofluids.

The effective density of nanofluids is defined by:

$$\rho_{ef} = (1 - \alpha) \rho_f + \alpha \rho_s. \quad (6)$$

The heat capacity of the nanofluid is expressed as follows:

$$(\rho c_p)_{ef} = (1 - \alpha) (\rho c_p)_f + \alpha (\rho c_p)_s. \quad (7)$$

For determining the effective viscosity, the Brinkman formulation is utilized:

$$\mu_{ef} = \frac{\mu_f}{(1-\alpha)^{2.5}} \text{ or } \mu_{ef} = (1-\alpha)\mu_f + \alpha\mu_s. \quad (8)$$

The effective thermal conductivity is simulated, following Chakraborty and Roy [50] as:

$$k_{ef} = k_{static} + k_{Brownian}, \quad (9)$$

$$\text{where, } k_{static} = k_f \left[ \frac{\frac{k_s}{k_f} + (n-1) \left\{ 1 + \left( \frac{k_s}{k_f} - 1 \right) \alpha \right\}}{\frac{k_s}{k_f} + (n-1) - \left( \frac{k_s}{k_f} - 1 \right) \alpha} \right]. \quad (10)$$

Here  $\alpha$  represents the nanoparticle volume fraction, the subscript  $s$  refers to the solid particle phase dispersed in the nanofluid, the subscript  $f$  refers to the property of a pure fluid devoid of any nano-particle suspensions and  $n$  is a shape factor to account for the differences in the shape of the particles (for spherical particles  $n=3$ ). For the Brownian component, invoking the kinetic theory and also Stokes' flow approximations, one may write:

$$k_{Brownian} = 5 \times 10^4 \beta \alpha (\rho c_p)_f \sqrt{\frac{k_B T}{\rho_s d_p}} f(\alpha, T), \quad (11)$$

where  $d_p$  represents the nanoparticle diameter,  $k_B$  is Boltzmann constant and  $\beta$  and  $f(\alpha, T)$  are expressed as:

$$\begin{aligned} \beta &= 0.0137(10\alpha)^{-1.6458}, \alpha < 1\% \\ &= 0.0011(10\alpha)^{-1.4544}, \alpha \geq 1\% \end{aligned} \quad \text{and}$$

$$f(\alpha, T) = (-6.04\alpha + 0.4705)T + (1722.3\alpha - 134.63), \text{ for } 1\% \leq \alpha \leq 4\%, 300\text{K} \leq T \leq 400\text{K}. \quad (12)$$

There is an enhancement of electrolyte concentration in the bulk fluid such that the electrical conductivity of the dispersion medium is increased from its base state. This augmentation of electrical conductivity is expected to alter the Joule heating to a significant extent and is expressed again following Chakraborty and Roy [50] as:

$$\sigma_{eff} = \sigma_f + \alpha(f - \sigma_s), \quad (13)$$

where,

$$f = \frac{12n_1e}{\kappa d_p} \left[ \left( e^{-e\zeta/(2k_B T)} - 1 \right) m^+ - \left( e^{e\zeta/(2k_B T)} - 1 \right) m^- - \frac{4}{\kappa d_p} \tanh\left(\frac{e\zeta}{4k_B T}\right) (m^+ + m^-) \right] + \frac{6Q_p m_p}{\pi d_p^3}, \quad (14)$$

here,  $m_p$  is the particle electrophoretic mobility,  $n_1$  is the equilibrium number concentration of the ions in the electrolyte solution and  $m^\pm$  are the mobilities of the positive/ negative ions. The charge on each particle,  $Q_p$ , is expressed as:

$$Q_p = \pi d_p^2 \frac{2k_B T \kappa \epsilon_s}{e} \sinh\left(\frac{e\zeta}{2k_B T}\right). \quad (15)$$

The electric potential,  $\bar{\Phi}$ , within the microchannel is modelled with the well-known Poisson-Boltzmann equation:

$$\nabla^2 \bar{\Phi} = -\frac{\bar{\rho}_e}{\epsilon_{ef}}, \quad (16)$$

where  $\bar{\rho}_e = ez(\bar{n}^+ - \bar{n}^-)$  is the electrical charge density,  $\bar{n}_+$  and  $\bar{n}_-$  are positive and negative ions having bulk concentration (number density)  $n_0$  and a valence of  $z_+$  and  $z_-$  respectively, and  $e$  represents elementary charge. Here,  $\epsilon_{ef}$  is the permittivity of the medium and it is defined for composite medium, according to Chakraborty and Roy [50] by the following relation:

$$\epsilon_{ef} = \epsilon_f + 3\alpha\epsilon_f \left( \frac{\epsilon_s - \epsilon_f}{\epsilon_s + 2\epsilon_f - \alpha(\epsilon_s - \epsilon_f)} \right). \quad (17)$$

Further, in order to determine the *electrical potential distribution*, it is necessary to describe the charge number density. For this, the *ionic number distributions* of the individual species are given by the Nernst-Planck equation for each species as:

$$\frac{\partial \bar{n}_\pm}{\partial t} + (\mathbf{q} \cdot \nabla) \bar{n}_\pm = D \nabla^2 \bar{n}_\pm \pm \frac{Dze}{k_B T} (\nabla \cdot (\bar{n}_\pm \nabla \bar{\Phi})), \quad (18)$$

where, we have assumed equal ionic diffusion coefficients for both the species, and that the mobility of the species is given by the Einstein formula and  $D$  represents the

diffusivity of the chemical species. It is pertinent to normalize the conservation equations. We therefore introduce the following non-dimensional parameters:

$$x = \frac{\bar{x}}{\lambda}, y = \frac{\bar{y}}{a}, t = \frac{c\bar{t}}{\lambda}, u = \frac{\bar{u}}{c}, v = \frac{\bar{v}}{c\delta}, h = \frac{\bar{h}}{a}, p = \frac{\bar{p}a^2}{\mu_{ef}c\lambda}, \phi = \frac{\bar{\phi}}{a}, \Phi = \frac{\bar{\Phi}}{\zeta}, n = \frac{\bar{n}}{n_0}. \quad (19)$$

Here  $x$  and  $y$  are dimensionless  $\bar{x}, \bar{y}$  coordinates,  $t$  is dimensionless time,  $u$  and  $v$  are dimensionless axial and transverse velocity components,  $h$  is non-dimensional transverse wall displacement,  $p$  is dimensionless pressure,  $\phi$  is dimensionless peristaltic wave amplitude,  $\Phi$  is dimensionless electric potential and  $n$  is dimensionless bulk concentration (number density) of the ions in the electrolyte. It is important to note that the *nonlinear* terms in the Nernst Planck equations are  $O(Pe\delta^2)$ , where  $Pe = ReSc$  represents the ionic Peclet number and  $Sc = \mu_{ef}/\rho_{ef}D$  denotes the Schmidt number. Therefore, the nonlinear terms may be dropped in the limit that  $Re, Pe, \delta \ll 1$  where

$$Re = \frac{\rho_{ef}ca\delta}{\mu_{ef}}$$
 is the Reynolds number and  $\delta = \frac{a}{\lambda}$  wave number. In this limit the Poisson-

Boltzmann equation is reduced to:

$$\frac{\partial^2 \Phi}{\partial y^2} = -\kappa^2 \left( \frac{n_+ - n_-}{2} \right), \quad (20)$$

where  $\kappa = aeZ \sqrt{\frac{2n_0}{\epsilon_{ef} K_B T}} = \frac{a}{\lambda_d}$ , is the Debye-Huckle parameter which defines the characteristic thickness of electrical double layer (EDL). The ionic distribution may be determined by means of the simplified Nernst Planck equations:

$$0 = \frac{\partial^2 n_{\pm}}{\partial y^2} \pm \frac{\partial}{\partial y} \left( n_{\pm} \frac{\partial \Phi}{\partial y} \right), \quad (21)$$

subjected to  $n_{\pm} = 1$  at  $\Phi = 0$  and  $\partial n_{\pm} / \partial y = 0$  where  $\partial \Phi / \partial y = 0$  (bulk conditions). These yield the much celebrated Boltzmann distribution for the ions:

$$n_{\pm} = e^{\mp \Phi}. \quad (22)$$

Combining Eqs. (20) and (22), we obtain the Poisson-Boltzmann paradigm for the electrical potential distribution in the electrolyte:

$$\frac{\partial^2 \Phi}{\partial y^2} = \kappa^2 \sinh(\Phi). \quad (23)$$

In order to make further analytical progress, we must simplify equation (23). Eq. (23) may be linearized under the low-zeta potential approximation. This assumption is not *ad hoc* since for a wide range of pH, the magnitude of zeta potential is less than 25 mV. It follows that Eq. (23) can be simplified to:

$$\frac{\partial^2 \Phi}{\partial y^2} = \kappa^2 \Phi, \quad (24)$$

which may be solved subjected to  $\frac{\partial \Phi}{\partial y} \Big|_{y=0} = 0$  and  $\Phi \Big|_{y=h} = 1$ , the potential function is

obtained as:

$$\Phi = \frac{\cosh(\kappa y)}{\cosh(\kappa h)}. \quad (25)$$

To quantify the relative order of volumetric heat generation due to electric resistance heating (Joule electro-thermal heating), and a local volumetric heating due to viscous dissipation, one may obtain a ratio of strength of Joule heating and viscous dissipation as:  $R_v \sim \frac{\sigma_f a \mu_f}{\kappa \epsilon_f^2 \zeta^2}$ . We may consider the viscous dissipation is negligible in comparison to

Joule heating effects for channel width greater than 10  $\mu\text{m}$ , as documented by Chakraborty and Roy [50]. Furthermore employing lubrication theory (neglecting inertial effects), the nonlinear terms in the momentum equation are found to be  $O(Re \delta^2)$  where  $Re$  is Reynolds number and  $\delta$  is the ratio of the transverse length scale to the axial length scale. These nonlinear terms can therefore be neglected. The emerging linearized conservation equations for mass, axial momentum, energy (heat) and solute concentration then assume the form:

$$\frac{\partial u}{\partial x} + \frac{\partial v}{\partial y} = 0, \quad (26)$$

$$\frac{\partial p}{\partial x} = \frac{\partial^2 u}{\partial y^2} + Gr_t T + Gr_c C + \kappa^2 U_{HS} \Phi, \quad (27)$$

$$\frac{\partial^2 T}{\partial y^2} + N_{tc} \frac{\partial^2 C}{\partial y^2} + S = 0, \quad (28)$$

$$\frac{\partial^2 C}{\partial y^2} + N_{ct} \frac{\partial^2 T}{\partial y^2} = 0, \quad (29)$$

where,  $Gr_t = \frac{\beta_t g \rho_{ef}^2 a^3 (T_1 - T_0)}{\mu_{ef}^2}$  and  $Gr_c = \frac{\beta_c g \rho_{ef}^2 a^3 (C_1 - C_0)}{\mu_{ef}^2}$  are the thermal and solutal

Grashof numbers,  $T = \frac{\bar{T} - T_0}{T_1 - T_0}$  and  $C = \frac{\bar{C} - T_0}{T_1 - T_0}$  are the dimensionless temperature and

solute concentration,  $N_{tc} = \frac{(\rho c_p)_{ef} D_{tc} (C_1 - C_0)}{k_{ef} (T_1 - T_0)}$  and  $N_{ct} = \frac{D_{ct} (T_1 - T_0)}{D_s (C_1 - C_0)}$  are the Dofour

thermo-diffusive and Soret diffuso-thermo parameters,  $U_{HS} = -\frac{E_x \varepsilon_{ef} \zeta}{\mu_{ef} c}$  is the Helmholtz-

Smoluchowski velocity (i.e. maximum electro-osmotic velocity) and

$S = \sigma_{ef} E_x^2 a^2 / k_{ef} (T_1 - T_0)$  is the normalized generation term that represents the ratio of Joule heating to surface heat flux (for constant wall temperature). The associated imposed boundary conditions at the micro-channel walls are:

$$T|_{y=0} = 0, T|_{y=h} = 1, C|_{y=0} = 0, C|_{y=h} = 1, \left. \frac{\partial u}{\partial y} \right|_{y=0} = 0, u|_{y=h} = 0. \quad (30)$$

The solutions of simultaneous partial differential equations (28) and (29) using the boundary conditions (30), are obtained as:

$$C = \frac{y}{h} + \frac{N_{ct} S (hy - y^2)}{2(-1 + N_{ct} N_{tc})}, \quad (31)$$

$$T = \frac{y}{h} + \frac{S(y^2 - hy)}{2(-1 + N_{ct} N_{tc})}. \quad (32)$$

Using Eqs. (31 & 32) in Eq. (27), and integrating Eqn. (27) with respect to  $y$  with the boundary condition (30), the *axial velocity* is obtained as:

$$u = \frac{1}{2} \frac{\partial p}{\partial x} (y^2 - h^2) + \frac{Gr_c + Gr_t}{8h} (h^3 - y^3) + \frac{S(Gr_c N_{ct} - Gr_t)}{24(-1 + N_{ct} N_{tc})} (h^4 - 2hy^3 + y^4) + U_{HS} \left\{ 1 - \frac{\cosh(\kappa y)}{\cosh(\kappa h)} \right\} \quad (33)$$

Volumetric flow rate is defined as  $Q = \int_0^h u dy$ , which when integrated, in view of Eq.(33),

takes the form:

$$Q = -\frac{h^3}{3} \frac{\partial p}{\partial x} + \frac{h^3}{8} (Gr_c + Gr_t) - \frac{7h^5 (Gr_t - Gr_c N_{ct}) S}{240(-1 + N_{ct} N_{tc})} + U_{HS} \left\{ h - \frac{\tanh(\kappa h)}{\kappa} \right\}. \quad (34)$$

Rearranging the terms of Eq. (34), the *pressure gradient* is obtained as:

$$\frac{\partial p}{\partial x} = -\frac{3Q}{h^3} + \frac{3}{8} (Gr_c + Gr_t) - \frac{7h^2 (Gr_t - Gr_c N_{ct}) S}{80(-1 + N_{ct} N_{tc})} + \frac{3U_{HS}}{h^3} \left\{ h - \frac{\tanh(\kappa h)}{\kappa} \right\}. \quad (35)$$

The *pressure difference across one wavelength* is defined as:

$$\Delta p = \int_0^1 \frac{\partial p}{\partial x} dx. \quad (36)$$

The transformations in non-dimensional form between the wave frame  $(x_w, y_w)$  moving with velocity  $(c)$  and the fixed (laboratory) frame  $(x, y)$  are given by:

$$x = x_w - t, \quad y = y_w, \quad u = u_w + 1, \quad v = v_w, \quad (37)$$

where  $(u_w, v_w)$  and  $(u, v)$  are the velocity components in the wave and fixed frame respectively.

The *volumetric flow rate in the wave frame* is given by

$$q_w = \int_0^h u_w dy_w = \int_0^h (u - 1) dy_w, \quad (38)$$

which, on integration, yields:

$$q_w = Q - h. \quad (39)$$

Averaging *volumetric flow rate* along one time period, we get:

$$\bar{Q} = \int_0^1 Q dt = \int_0^1 (q_w + h) dt, \quad (40)$$

Integrating Eq. (40) yields:

$$\bar{Q} = q_w + 1 - \phi / 2 = Q + 1 - h - \phi / 2. \quad (41)$$

Using Eqs. (33), the stream function in the wave form (obeying the Cauchy-Riemann

equations,  $u_w = \frac{\partial \psi}{\partial y_w}$  and  $v_w = -\frac{\partial \psi}{\partial x_w}$ ) takes the form:

$$\psi = \frac{\bar{Q}-1+\phi/2+h}{2h^3}(3h^2y-y^3) + \frac{a_{11}U_{HS}}{2} + (Gr_t a_{12} - Gr_c a_{13}) \frac{yh^2(h-y)^2}{480h^3(-1+N_{ct}N_{tc})}. \quad (42)$$

Here the following definitions apply:

$$a_{11} = -y + \frac{y^3}{h^2} + \frac{1}{\kappa} \left( \frac{(3h^2 - y^2) \tanh(\kappa h)}{h^3} - \frac{2 \sinh(\kappa y)}{\cosh(\kappa h)} \right), \quad (43a)$$

$$a_{12} = hS(h^2 + 2hy - 4y^2) - 10(N_{ct}N_{tc} - 1)(2y + h), \quad (43b)$$

$$a_{13} = hN_{ct}S(h^2 + 2hy - 4y^2) + 10(N_{ct}N_{tc} - 1)(2y + h). \quad (43c)$$

Key engineering design parameters at the micro-channel walls are the skin friction coefficient ( $C_f$ ) i.e. surface shear stress function, Nusselt number ( $N_u$ ) i.e. wall heat transfer rate and also the Sherwood number ( $S_h$ ) i.e. the wall solute mass (species) gradient. These are defined respectively for the present regime as:

$$C_f = \left. \frac{\partial h}{\partial x} \frac{\partial u}{\partial y} \right|_{y=h} \quad (44)$$

$$N_u = \left. \frac{\partial h}{\partial x} \frac{\partial \theta}{\partial y} \right|_{y=h}. \quad (45)$$

$$S_h = \left. \frac{\partial h}{\partial x} \frac{\partial C}{\partial y} \right|_{y=h} \quad (46)$$

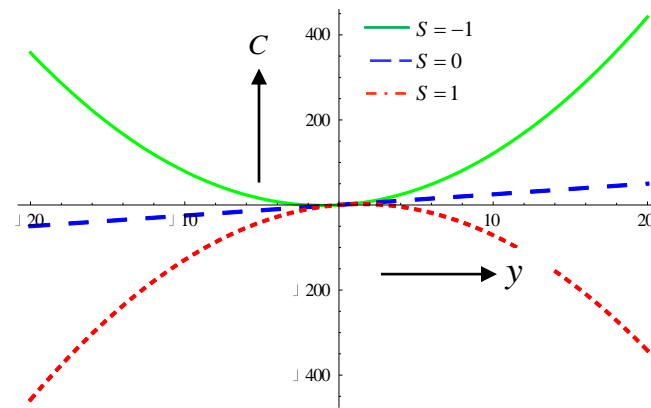
### 3. NUMERICAL RESULTS AND DISCUSSION

The present boundary value problem is clearly dictated by a number of thermal, electrical and nanofluidic parameters. For the purposes of brevity, we consider the influence of two parameters on peristaltic flow characteristics, specifically the Joule heating parameter ( $S$ ) and the Helmholtz-Smoluchowski velocity ( $U_{HS}$ ). The effect of Joule heating parameter will be proportional to the effect of the nanoparticle volume fraction and also proportional to the diameter of nanoparticles ( $S = \sigma_{ef} E_x^2 a^2 / k_{ef} (T_1 - T_0)$ ) where,

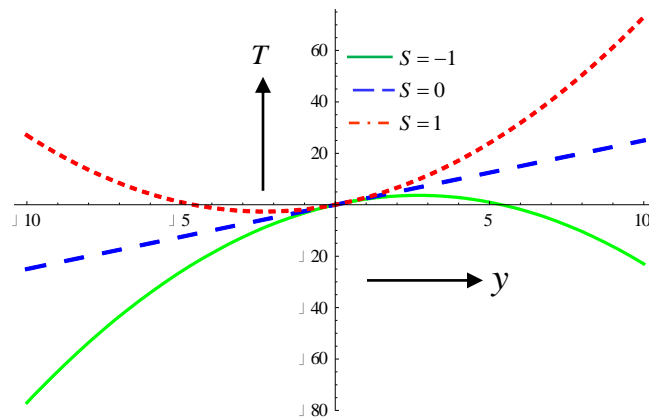
$$\sigma_{eff} = \sigma_f + \alpha(f - \sigma_s) \quad \text{and} \quad k_{ef} = k_{static} + 5 \times 10^4 \beta \alpha (\rho c_p)_f \sqrt{\frac{k_B T}{\rho_s d_p}} f(\alpha, T). \quad \text{However nano-}$$

particle geometry effects are not explicitly considered here and will be addressed in future studies.

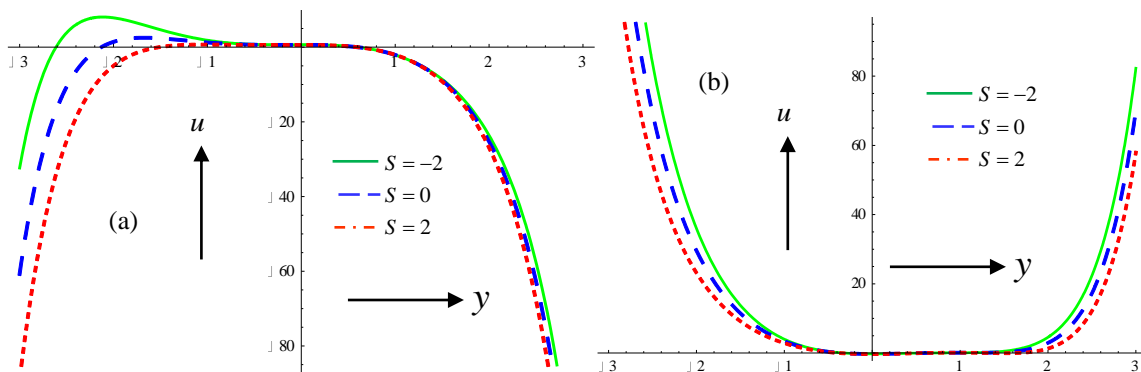
Figs. 2 to 12 illustrate the effects of these two selected parameters on key characteristics including temperature, velocity, pressure, solute concentration and streamline distributions. Generally in these figures the following default values are prescribed:  $\phi = 0.4$ ,  $p_x = 1$ ,  $N_{ct} = 1$ ,  $N_{tc} = 2$ ,  $Gr_c = 1$ ,  $Gr_t = 5$ ,  $\kappa = 2$ . Therefore in all plots thermal and species buoyancy are present and also the cross-diffusion (Soret and Dufour phenomena) are significant. A constant axial pressure gradient scenario is considered and a finite thickness of the Debye electrical double layer.



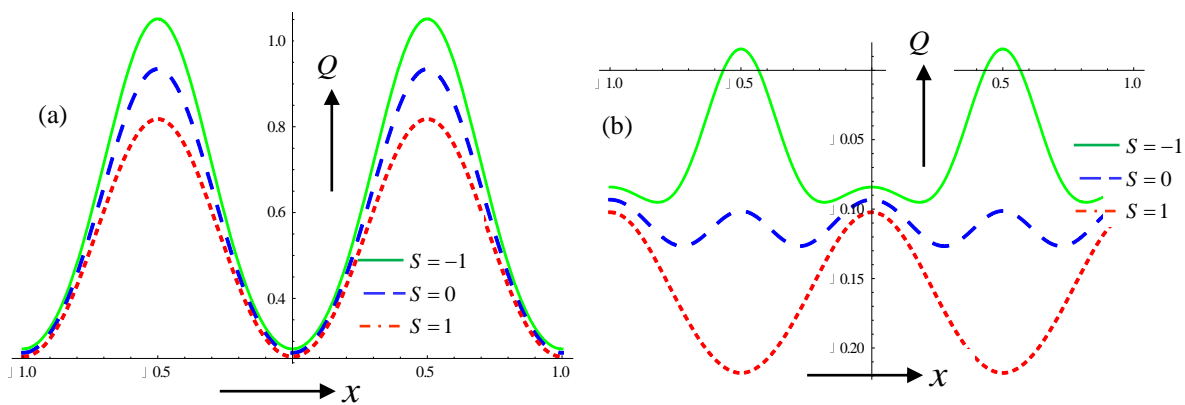
**Fig.2.** Solute concentration profile at  $\phi = 0.6$ ,  $N_{ct} = 2$ ,  $N_{tc} = 1$  for different values of Joule heating parameter.



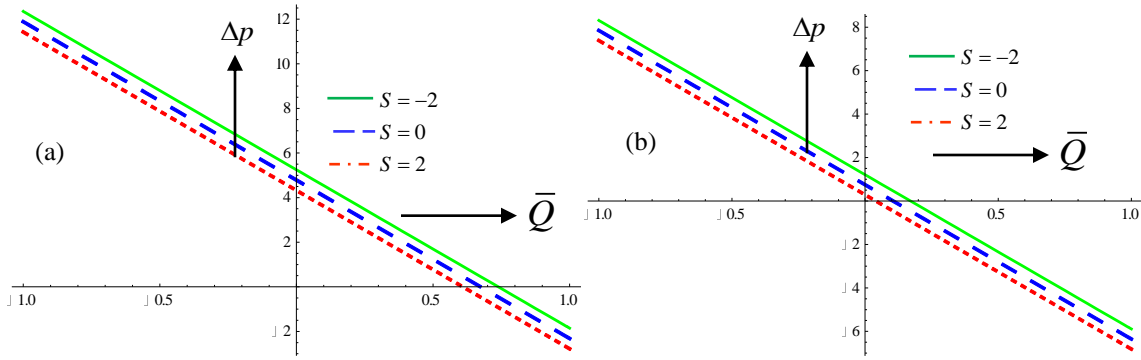
**Fig.3.** Temperature profile at  $\phi = 0.6$ ,  $N_{ct} = 2$ ,  $N_{tc} = 1$  for different values of Joule heating parameter.



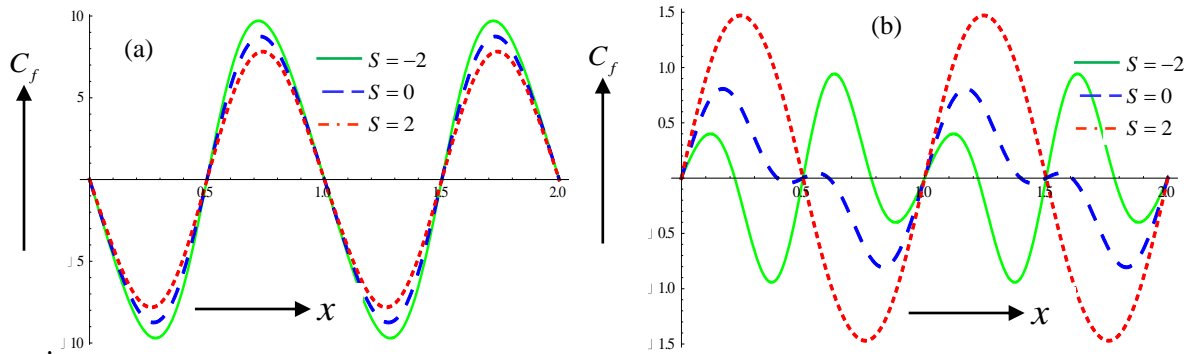
**Fig.4.** Velocity profile at  $\phi = 0.4, p_x = 1, N_{ct} = 1, N_{tc} = 2, Gr_c = 1, Gr_t = 5, \kappa = 2$  for different values of Joule heating parameter (a)  $U_{HS} = 1$  (b)  $U_{HS} = -1$ .



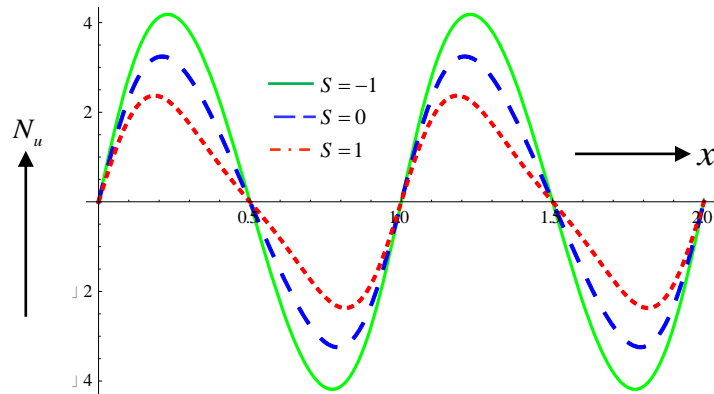
**Fig.5.** Volumetric flow rate along the channel length at  $\phi = 0.4, p_x = 1, N_{ct} = 1, N_{tc} = 2, Gr_c = 1, Gr_t = 5, \kappa = 2$  for different values of Joule heating parameter (a)  $U_{HS} = 1$  (b)  $U_{HS} = -1$ .



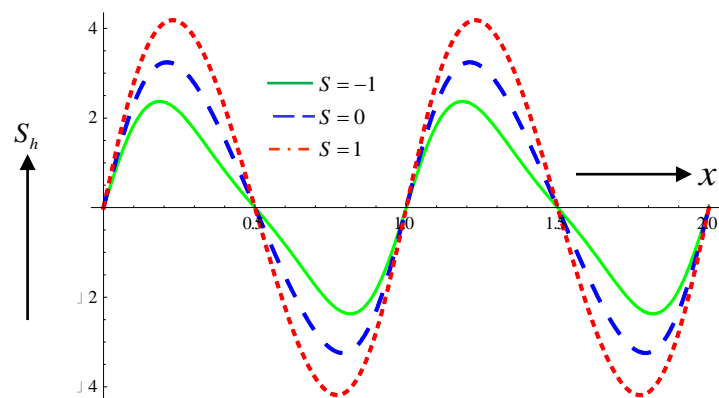
**Fig.6.** Pressure across one wavelength vs time averaged volumetric flow rate at  $\phi = 0.4$ ,  $N_{ct} = 1, N_{tc} = 2$ ,  $Gr_c = 1, Gr_t = 5$ ,  $\kappa = 2$  for different values of Joule heating parameter (a)  $U_{HS} = 1$  (b)  $U_{HS} = -1$ .



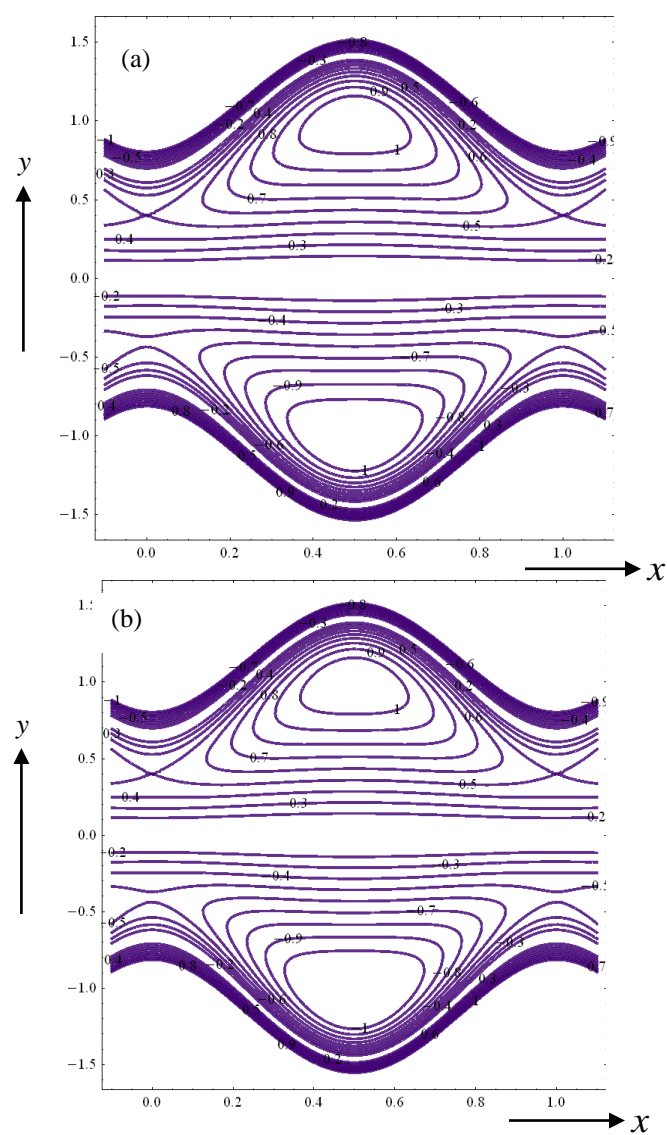
**Fig.7.** Skin friction coefficient along the channel length at  $\phi = 0.4$ ,  $p_x = 1, N_{ct} = 1, N_{tc} = 2$ ,  $Gr_c = 1, Gr_t = 5$ ,  $\kappa = 2$  for different values of Joule heating parameter. (a)  $U_{HS} = 1$  (b)  $U_{HS} = -1$ .

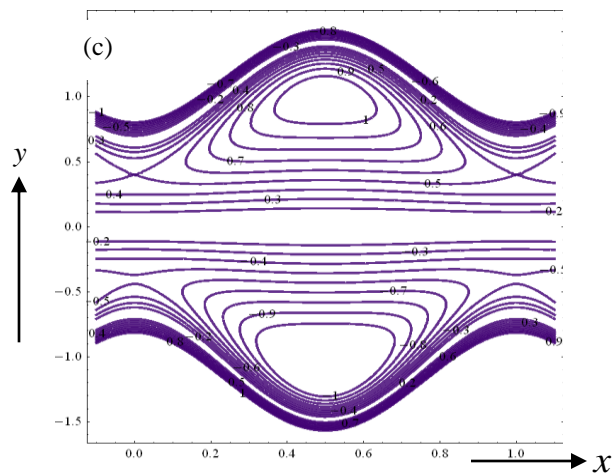


**Fig.8.** Nusselt number along the channel length at  $\phi = 0.4, N_{ct} = 1, N_{tc} = 2$  for different values of Joule heating parameter.

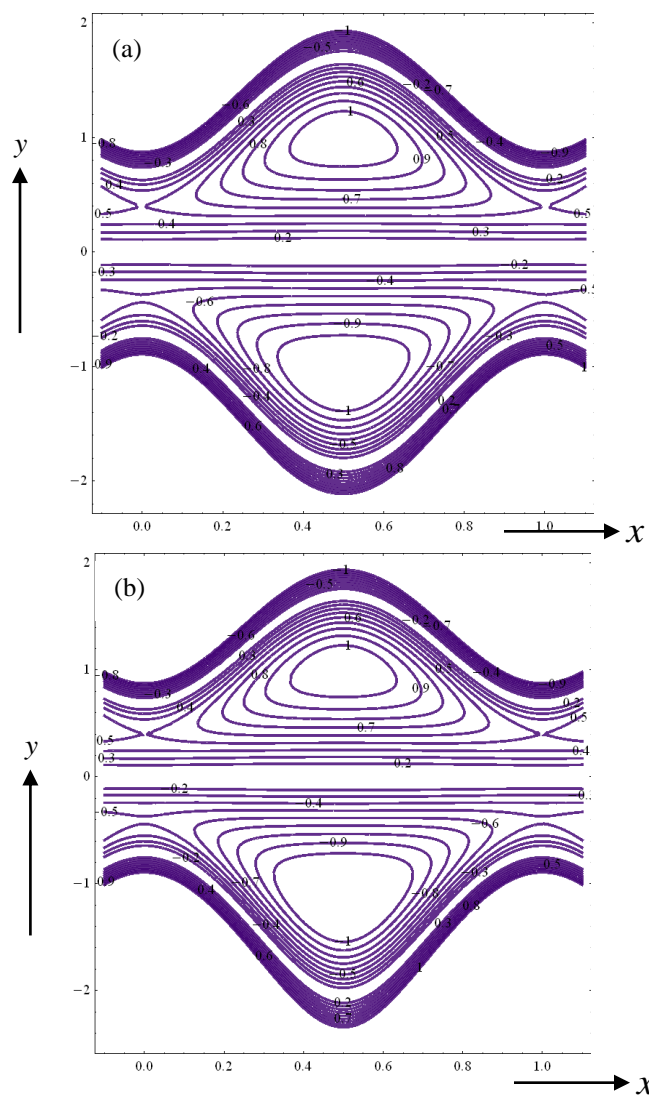


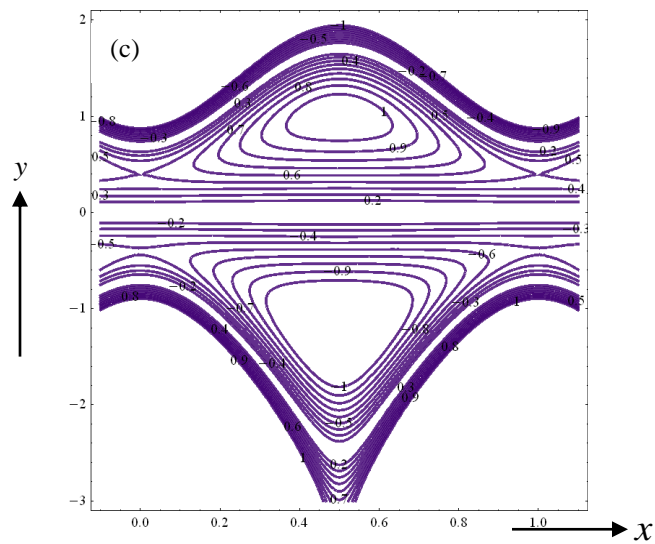
**Fig.9.** Sherwood number along the channel length at  $\phi = 0.4, N_{ct} = 1, N_{tc} = 2$  for different values of Joule heating parameter.



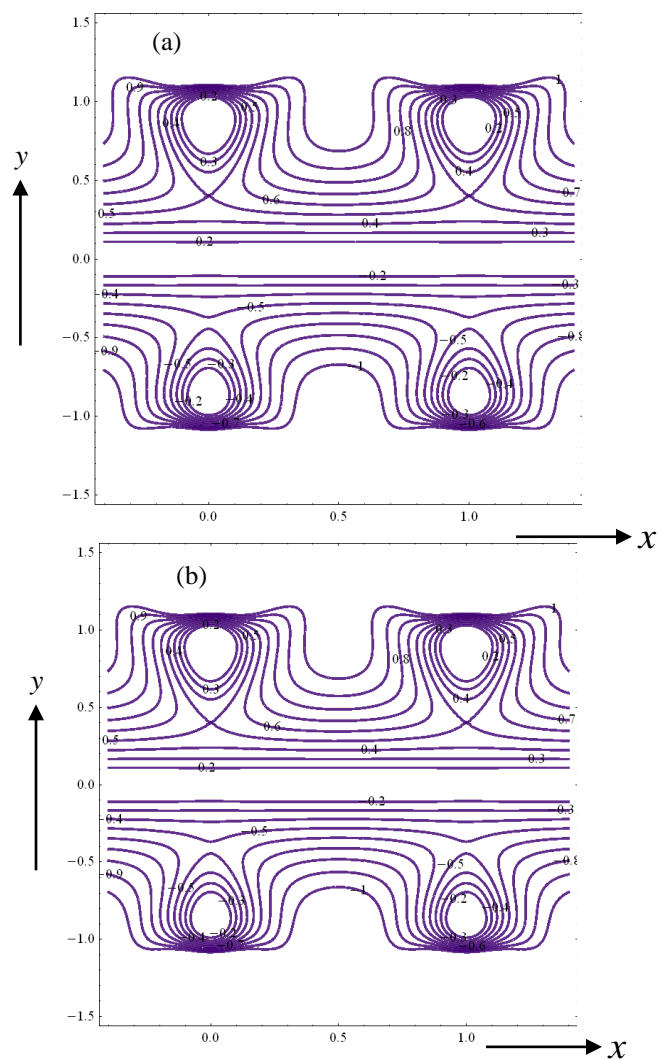


**Fig.10.** Stream lines at  $U_{HS}=1, \phi=0.6, \bar{Q}=0.8, N_{ct}=1, N_{tc}=2, Gr_c=1, Gr_t=0.1, \kappa=5$  for (a)  $S=-1$ , (b)  $S=0$ , (c)  $S=1$ .





**Fig.11.** Stream lines at  $U_{HS}=0, \phi=0.6, \bar{Q}=0.8, N_{ct}=1, N_{tc}=2, Gr_c=1, Gr_t=0.1, \kappa=5$  (a)  $S=-1$ (b) $S=0$ (c) $S=1$



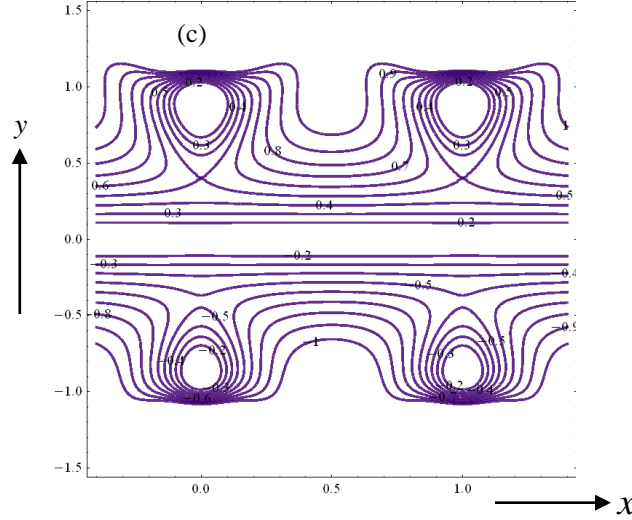


**Fig.12.** Stream lines at  $U_{HS} = -1, \phi = 0.6, \bar{Q} = 0.8, N_{ct} = 1, N_{tc} = 2, Gr_c = 1, Gr_t = 0.1, \kappa = 5$  (a)  $S = -1$  (b)  $S = 0$  (c)  $S = 1$ .

**Fig. 2** presents the solute concentration distribution ( $C$ ) with Joule heating parameter ( $S$ ). With negative values of  $S$  concentrations are generally enhanced (and positive) whereas with positive values of  $S$  they are reduced (and negative). The presence of an applied voltage gradient and its induced electric conduction results in Joule electro-thermal heating in the electrolyte. For  $S < 0$  this results in volumetric energy generation in the electro-osmotic flow. However for  $S > 0$  energy is extracted from the flow. Negative values of  $S$  therefore encourage nano-particle species diffusion in the regime and this elevates  $C$  values. The reverse effect is induced with positive  $S$  values. It is also noteworthy that non-zero values of Joule heating result in parabolic distributions, whereas zero value manifests in a linear profile of solute concentration across the micro-channel span. Evidently a substantial modification in the diffusion of nano-particles is generated via Joule heating, implying in turn that axial electrical field (since  $S = \sigma_{ef} E_x^2 a^2 / k_{ef} (T_1 - T_0)$ ) has a marked influence in controlling the organization of nano-particles in the flow. Although the Joule parameter,  $S$ , does not arise in the species conservation eqn. (29), the Soret thermo-diffusive term  $N_{ct} \frac{\partial^2 C}{\partial y^2}$  in Eq.(29) couples the solute concentration ( $C$ ) with the temperature field i.e. Eq.(28) and therefore the influence of Joule heating is exerted indirectly on the nano-particle diffusion. Much

higher values are computed for concentration at the upper channel all as compared with the lower channel wall, irrespective of the Joule heating effect. These observations generally concur with the rigid micro-channel study conducted by Chakraborty and Roy [50].

**Fig. 3** illustrates the response in temperature field,  $T$ , to variation in Joule heating parameter ( $S$ ), across the micro-channel. It is apparent that negative values of  $S$ , induces a cooling in the electrolyte i.e. decreases temperatures and constrains them to be generally negative. The converse response is induced with positive values of  $S$ . In short the response of temperature field to electrical Joule heating is the opposite of that exhibited by the solute concentration field (Fig. 2). The transverse heat conduction term in the

energy eqn. (28) i.e.  $\frac{\partial^2 T}{\partial y^2}$  is directly modified by the magnitude and sign of the Joule

parameter,  $S$ . Again the case of  $S = 0$  (absence of Joule heating) results in a linear profile for temperature. Temperatures are clearly maximized near the upper channel wall for positive Joule heating and minimized near the lower wall for negative Joule heating. Similar results have been reported by for example Sadeghi *et al.* [49]. It is also worthy to note that the low Péclet number assumed in the present analysis, encourages back diffusion of heat from the entry zone to the exit zone of the channel and this in turn does modify the transverse distributions of temperature, as reported by among others, Petersen *et al.* [48].

**Figs. 4a,b** presents the evolution in axial velocity in the micro-channel with a change in electro-thermal Joule parameter,  $S$ , for two different values of Helmholtz-Smoluchowski velocity ( $U_{HS}$ ). Fig.4a shows that generally inverted plug flow profiles are computed across the channel with maximum values towards the core zone and a significant drop off towards the charge-carrying walls, with  $U_{HS} = 1$ . Negative Joule heating generates a notable acceleration across the channel whereas positive Joule heating manifests in a marked deceleration. However in the central zone there is very little difference computed with changing electrical field i.e. a change in  $S$  since the ionic charges are localized at the walls and not in the bulk of the fluid. The presence of the negative ion charges on the wall surfaces creates a concentration gradient of positively charged ions near the wall surfaces, but no tangible injection of charges along the central line of the channel. This

results in an electrical potential distribution in the electrolyte which is known as the electric double layer (EDL). When electrical field (axial) is increased i.e. with greater Joule parameter (for constant temperature difference), the electro-kinetic body force (in the momentum eqn. (27) i.e.  $+\kappa^2 U_{HS} \Phi$ ) is also enhanced. The change is assistive for negative  $S$  values and inhibitive for positive  $S$  values resulting respectively in acceleration or deceleration of the axial flow. Clearly the Joule parameter instigates a considerable modification in flow distribution across the channel and confirms the excellent ability of electro-osmotic phenomena in regulating velocity profiles at the micro-channel walls. Fig.4b exhibits very different distributions for the flow velocity with  $U_{HS} = -1$ . Generally positive magnitudes are computed across the channel space and the maximum velocity arises at the channel walls with a minimum at the central core zone of the channel. With negative Joule heating parameter,  $S$ , higher magnitudes are computed and vice versa for positive  $S$  values. Axial electrical field therefore exerts a similar influence on velocity distributions irrespective of whether *Helmholtz-Smoluchowski velocity* ( $U_{HS}$ ) is positive or negative; however for positive  $U_{HS}$  velocity is generally negative whereas for negative  $U_{HS}$  velocity is overwhelmingly positive.

**Figs. 5a,b** depicts the profiles of volumetric flow rate ( $Q$ ) with axial coordinate with different values of Joule heating parameter values ( $S$ ), again for two different values of *Helmholtz-Smoluchowski velocity* ( $U_{HS}$ ). Both graphs are again plotted at  $t = 0.48$ . The axial flow acceleration with greater electrical field and therefore larger negative  $S$  values (as witnessed in fig. 4) serves to enhance flow rates. This results in an elevation in  $Q$  values for  $S < 0$  and a reduction in  $Q$  values for  $S > 0$  (the case of  $S=0$  which corresponds to an absence of Joule heating is intercalated between these two other cases). The periodic nature of the flow is clearly captured in Fig.5a and is associated with peristaltic wave propagation. The alternating peaks and troughs exhibit consistent magnitudes with axial distance i.e. there is no alteration in magnitudes with distance along the channel. Fig.5b presents the volumetric flow rate profiles with  $U_{HS} = -1$ , and significantly different behaviour is observed compared with fig. 5a. With any  $S$  value the volumetric flow rates remain now generally negative i.e. reversed flow. However positive values are achieved for small sections of the channel width with  $S = -1$ . Greater periodicity of the flow is also induced with

negative Helmholtz-Smoluchowski velocity ( $U_{HS}$ ) as shown in Fig.5b, compared with positive Helmholtz-Smoluchowski velocity ( $U_{HS}$ ) (Fig.5a). With vanishing Joule parameter ( $S=0$ ), the number of peaks and troughs is maximized in Fig.5b.

**Figs. 6a, b** presents the evolution in pressure difference across one wavelength ( $\Delta p$ ) with time averaged volumetric flow rate ( $\bar{Q}$ ) for various Joule heating parameter values ( $S$ ). Three pumping regimes can be classified. These are the pumping region ( $\Delta p > 0$ ), the augmented pumping region ( $\Delta p < 0$ ), and the free pumping region ( $\Delta p = 0$ ). Generally in the pumping region pressure difference rises with negative flow rates whereas it decreases with positive flow rates. Fig.6a shows that there is overall an inverse linear relationship between pressure difference and time averaged flow rate. For positive values of Joule heating ( $S$ ), pressure difference is observed to be elevated at all flow rates. Conversely with negative values of Joule heating, the pressure difference is suppressed over the entire range of values of  $\bar{Q}$ . Fig.6b demonstrates that while a linear relationship is again apparent for pressure difference and time averaged flow rate, with negative Helmholtz-Smoluchowski velocity ( $U_{HS}$ ), the magnitudes of pressure difference are somewhat reduced. The linear decays for all values of  $S$  and pass much closer to the origina than for positive Helmholtz-Smoluchowski velocity ( $U_{HS}$ ), i.e. Fig. 6a.

**Fig. 7a,b** present the skin friction (wall shear stress function) distributions with axial coordinate for various Joule heating parameter values ( $S$ ). Evidently skin friction profiles are oscillatory in nature. Fig.7a, corresponding to positive Helmholtz-Smoluchowski velocity ( $U_{HS}$ ), show that the magnitudes of skin friction are elevated for negative  $S$  values (in consistency with the axial flow acceleration computed earlier in Fig. 4a) and decreased with positive  $S$  values (confirming the axial flow retardation in Fig.4a). Peaks and troughs are consistently maintained at similar magnitudes along the channel length i.e. they do not vary with distance along the channel  $x$ -axis. The influence of the sign of Joule heating is considerable. The results confirm that the primary influence of Joule heating (and axial electrical field) is confined to the walls of the micro-channel where charge concentration is maximized. This agrees also with other investigations, including Chakraborty [44] and also Bandopadhyay *et al.* [46]. Fig.7b shows that for negative Helmholtz-Smoluchowski velocity ( $U_{HS}$ ), skin friction magnitudes are elevated with

positive Joule heating parameter ( $S = 2$ ) whereas they are depressed with negative Joule heating parameter i.e. the opposite trend to Fig.7a. The smooth undulating profiles in Fig.7a for all values of  $S$  are only retained in Fig.7b for positive  $S$ . In Fig.7b the cases for  $S = 0, -2$  exhibit a modified structure with no consistency in peaks and troughs. Magnitudes of skin friction are also significantly lower in Fig.7b (positive  $U_{HS}$ ) than in Fig.7a (negative  $U_{HS}$ ).

**Fig.8** illustrates the evolution in Nusselt number profiles with axial coordinate for various Joule heating parameter values ( $S$ ). Nusselt number measures the heat transfer rate (temperature gradient) at the micro-channel walls and furthermore embodies the ratio of *thermal convective heat transfer* to *thermal conduction heat transfer*. With enhanced negative Joule heating ( $S < 0$ ), the Nusselt number is elevated at the peaks and decreased at the troughs. This agrees with the decrease in temperatures computed in Fig.3 and is caused by the enhanced diffusion of heat away from the fluid to the channel walls. Nusselt number is conversely depressed with positive values of Joule heating and this again agrees physically with the increase in temperatures computed in fig. 3. Higher temperatures in the micro-channel imply a migration of heat from the channel walls into the nanofluid. The impact of Joule heating is consistent for different  $x$ -values. These patterns are generally in agreement with earlier studies including Schit *et al.* [23].

**Fig. 9** presents the profiles for Sherwood number with axial coordinate for various Joule heating parameter values ( $S$ ). The dimensionless solute mass transfer rate (i.e. concentration gradient) at the channel walls is quantified with Sherwood number, which also measures the ratio of the convective mass transfer to the rate of diffusive mass transport. The response in Sherwood number to Joule electro-thermal parameter is opposite to that of the Nusselt number. Positive  $S$  values are observed to elevate  $Sh$  values (associated with decreasing concentrations in the nanofluid, as computed in Fig. 2) whereas negative  $S$  values induce a reduction in Sherwood numbers. Joule electro-thermal effect therefore modifies the solute diffusion rate significantly.

**Figs. 10-12** present the combined effects of the Helmholtz-Smoluchowski velocity ( $U_{HS}$ ) and Joule heating parameter ( $S$ ) on nanofluid bolus dynamics i.e. trapping phenomena. In these plots, Figs. 10a, 11a, 12a correspond to  $S = -1$  with  $U_{HS} = 1, 0$  and  $-1$ , respectively. Figs.10b, 11b, 12b correspond to  $S = 0$  with  $U_{HS} = 1, 0$  and  $-1$ , respectively. Figs 10c,

11c, 12c correspond to  $S = 1$  with  $U_{HS} = 1, 0$  and  $-1$ , respectively. An increase in Helmholtz-Smoluchowski velocity ( $U_{HS}$ ) implies an elevation in axial electrical field strength. This results in an intensification in the circulation as  $U_{HS}$  decreases from 1 (Fig. 10a) to 0 (Fig.11a) i.e. a closer proximity of streamlines. A significantly stronger circulation and the synthesis of a quadruple system of boluses however is induced with subsequent change in  $U_{HS}$  to  $-1$ , as seen in Fig.12a. Similar modifications are also observed in Figs. 10b, 11b, 12b ( $S= 0$ ) and also Figs.10c, 11c, 12c ( $S=1$ ). The influence of axial electrical field therefore is maximized with negative values of the electro-osmotic velocity. To expound the Joule heating effect, we consider Figs.10a-c, 11a-c and 12a-c. There is a weak modification in the trapping bolus structures computed for each of these sets of figures with increasing  $S$ , indicating that the Joule heating effect is secondary to the electro-osmotic velocity effect. In all the streamline plots assistive thermal and species buoyancy are present ( $Gr_c=Gr_t=1$ ) and of the same order of magnitude.

#### 4. CONCLUSIONS

A mathematical study has been conducted to investigate the influence of Joule electro-thermal heating in electro-kinetic nanofluid thermo-diffusive pumping via peristaltic wave motion in an isothermal finite length micro-channel under uniform axial electrical field. Soret and Dufour cross-diffusion effects and also thermal and species buoyancy effects have been incorporated. Integral solutions have been obtained for the non-dimensional linearized boundary value problem, under lubrication and Debye approximations. Mathematica software has been deployed to evaluate numerical solutions derived for solute concentration, axial velocity, temperature distribution, pressure difference, volumetric flow rate, skin friction (wall shear stress function), Nusselt number (wall temperature gradient) and Sherwood number (wall concentration gradient). Some important observations from these simulations may be summarized as follows:

- Increasing positive Joule parameter strongly suppresses solute concentrations whereas increasing negative Joule number results in a strong elevation in concentration.

- Increasing positive Joule parameter markedly enhances temperatures (i.e. induces micro-channel heating) whereas increasing negative Joule number significantly depress temperatures (i.e. manifest in cooling of the micro-channel).
- Increasing negative Joule parameter accelerates axial flow substantially whereas increasing positive Joule parameter decelerates the axial flow, and in both cases the effect is prominent near the micro-channel walls and is negligible in the core zone since the ionic charge distribution decreases from a maximum in the vicinity of wall (associated with the zeta potential) to negligible nanofluid charge in the core.
- Increasing negative Joule parameter values enhance volumetric flow rates whereas the converse behavior is induced with positive Joule heating values, and this pattern is sustained periodically along the channel length.
- Pressure differences are decreased with increasing time-averaged volumetric flow rate and also with positive Joule electro-thermal parameter values.
- Skin friction values are elevated with negative Joule parameter and reduced with positive Joule parameter.
- Nusselt number is increased with negative Joule heating effect (heating of the micro-channel walls), whereas it is significantly decreased with positive Joule heating effect (cooling of the micro-channel walls).
- Sherwood number is enhanced with positive Joule heating effect (heating of the micro-channel walls), whereas it is strongly suppressed with negative Joule heating effect (cooling of the micro-channel walls).
- With negative electro-osmotic velocity the dual bolus formation present for positive electro-osmotic velocity is further divided into a quadruple system of symmetrical boluses and the number of trapped fluid zones therefore increased.
- A change in Joule heating parameter weakly intensifies the circulation in the regime.

The present work has been confined to Newtonian nanofluid electrolytes. Future studies will consider non-Newtonian ionic liquids [39] e.g. viscoelastic characteristics, and will be communicated imminently. Furthermore it is hoped that the present work will

stimulate experimental studies in electro-kinetic nanofluid peristaltic pumping to explore further applications in technology.

## ACKNOWLEDGEMENTS

O. Anwar Bég wishes to express his deepest appreciation to the late *Tazzy Bég* (August 14<sup>th</sup> 2008-September 9<sup>th</sup> 2016) who brought so much contentment to his family life, who was the very best of companions and a tremendous inspiration for much of his academic efforts.

## REFERENCES

1. S.U.S. Choi, enhancing thermal conductivity of fluid with nanofluid, in: *D. A. Siginer, Wang HP (Eds.), Developments and Applications of non-Newtonian flows. ASME J Heat Transfer*, 66, 99–105. (1995).
2. R. Taylor et al., Small particles, big impacts: A review of the diverse applications of nanofluids, *J. Appl. Phys.* 113, 011301 (2013).
3. B.G. Wang, X.B. Wang, W.J. Lou, J.C. Hao, Rheological and tribological properties of ionic liquid-based nanofluids containing functionalized multi-walled carbon nanotubes, *J. Phys. Chem. C*, 114, 8749-8755 (2010).
4. G. Huminic and A. Huminic, Application of nanofluids in heat exchangers: A review, *Renewable and Sustainable Energy Reviews*, 16, 5625–5638 (2012).
5. L. Zhang *et al.*, The properties of ZnO nanofluids and the role of H<sub>2</sub>O<sub>2</sub> in the disinfection activity against *Escherichia coli*, *Water Res.*, 47 (12) 4013-21 (2013).
6. O. Anwar Bég, M. F. M. Basir, M.J. Uddin and A. I. M. Ismail, Numerical study of slip effects on unsteady aysmmetric bioconvective nanofluid flow in a porous microchannel with an expanding/ contracting upper wall using Buongiorno's model, *J. Mechanics in Medicine and Biology* (2016). 28 pages **DOI: <http://dx.doi.org/10.1142/S0219519417500592>**

7. D. Su, R. Ma, L. Zhu, Numerical study of nanofluid infusion in deformable tissues for hyperthermia cancer treatments, *Medical & Biological Engineering & Computing*, 49, 1233–1240 (2011).
8. C.T. Lim, J. Han, J. Guck and H. Espinosa, Micro and nanotechnology for biological and biomedical applications, *Med. Biol. Eng. Comp.*, 48 (10) 941–943 (2010).
9. D. Yadav, G.S. Agrawal and R. Bhargava, Thermal instability of rotating nanofluid layer, *Int. J. Engineering Science*, 49, 1171-1184 (2011).
10. M.F.M. Basir, M.J. Uddin, A.I.M. Ismail, A. I. M. and O. Anwar Bég, Unsteady bio-nanofluid slip flow over a stretching cylinder with bioconvection Schmidt and Péclet number effects, *AIP Advances*, 6, 055316-1 - 055316-15 (2016).
11. K. Zaimi, A. Ishak and I. Pop, Stagnation-point flow toward a stretching/shrinking sheet in a nanofluid containing both nanoparticles and gyrotactic microorganisms, *ASME J. Heat Transfer*, 36, 041705-1 (2014).
12. F.F. Reuss, Sur un nouvel e-et de l'électricité galvanique, *Mem. Soc. Imp. Nat. Mosc.*, 2, 327–337 (1809).
13. G. Luft, D. Kuehl, G.J. Richter, Electro-osmotic valve for the controlled administration of drugs, *Med. Biol. Eng. Comp.*, 16, 45–50 (1978).
14. M.J. Pikal, The role of electroosmotic flow in transdermal iontophoresis, *Adv. Drug Deliv. Rev.* 46, 281–305 (2000).
15. R. Shirsavar, A. Ramos, A. Amjadi, J. Taherinia, M. Mashhadi, A. Nejati, Induced soap-film flow by non-uniform alternating electric field, *J. Electrostatics*, 73, 112-116 (2015).
16. M.R. Bown and C.D. Meinhart, AC electroosmotic flow in a DNA concentrator, *Microfluid. Nanofluid.* 2, 513–523 (2006).
17. M. Dejam, H. Hassanzadeh, Z. Chen, Shear dispersion in combined pressure-driven and electro-osmotic flows in a channel with porous walls, *Chemical Engineering Science*, 137, 205-215 (2015).

18. E. Moreau, P.O. Grimaud, G. Touchard, Electrical decontamination of soil, *J. Electrostatics*, 40/41, 675-680 (1997).
19. Y. Jian *et al.*, Transient electroosmotic flow of general Maxwell fluids through a slit microchannel, *Zeitschrift für angewandte Mathematik und Physik*, 65, 435–447 (2014).
20. Y. Y. Liang, G. F. Weihs, R. Setiawan, D. Wiley, CFD modelling of unsteady electro-osmotic permeate flux enhancement in membrane systems, *Chemical Engineering Science*, 146, 189-198 (2016).
21. B.D. Iverson, D. Maynes and B.W. Webb, Thermally developing electro osmotic convection in rectangular micro channels with vanishing Debye layer thickness, *AIAA J Thermophysics and Heat Transfer*, 18, 486-496 (2004).
22. S. L. Broderick, B. W. Webb, D. Maynes, Thermally developing electro-osmotic convection in microchannels with finite Debye-layer thickness, *Numerical Heat Transfer, Part A: Applications*, 48, 941-964 (2005).
23. G.C. Schit, A. Mondal, A. Sinha and P.K. Kundu, Electro-osmotic flow of power-law fluid and heat transfer in a micro-channel with effects of Joule heating and thermal radiation, *Physica A: Statistical Mechanics and its Applications*, 462, 1040–1057 (2016).
24. S.M.S. Murshed, K.C. Leong, C. Yang, Thermophysical and electrokinetic properties of nanofluids – A critical review, *Applied Thermal Engineering*, 28, 2109–2125 (2008).
25. D. Dutta, A numerical analysis of nanofluidic charge based separations using a combination of electrokinetic and hydrodynamic flows, *Chemical Engineering Science*, 93, 124-130 (2013).
26. H. Safarnia, M. Sheikholeslami and D.D. Ganji, Electrohydrodynamic nanofluid flow and forced convective heat transfer in a channel, *Eur. Phys. J. Plus*, 131, 96-100 (2016).
27. C.J. Choi, S.P. Jang and S.U.S. Choi, Electrokinetic effects of charged nanoparticles in microfluidic Couette flow, *J. Colloid and Interface Science*, 363, 59–63 (2011).

28. H. B. Rokni, D. M. Alsaad and P. Valipour, Electrohydrodynamic nanofluid flow and heat transfer between two plates, *J. Molecular Liquids*, 216, 583-589 (2016).
29. Y.C. Fung and C.S. Yin, Peristaltic transport, *ASME J. Appl. Mech.*, 33, 669–675 (1968)..
30. M.Y. Jaffrin, A.H. Shapiro, Peristaltic pumping, *Ann. Rev. Fluid Mech.*, 3, 13–36 (1971).
31. H.C. Chang and G. Yossifon, Understanding electrokinetics at the nanoscale: a perspective, *Biomicrofluidics*, 3, 012001 (2009).
32. Y. Takamura, *et al.* Low-voltage electroosmosis pump for stand-alone microfluidics devices, *Electrophoresis*, 24, 185–192 (2003).
33. D.S. Reichmuth, Chirica, G. S. & Kirby, B. J. Increasing the performance of high-pressure, high-efficiency electrokinetic micropumps using zwitterionic solute additives. *Sens. Actuat. B*, 92, 37–43 (2003).
34. J.M. Berg *et al.*, A two-stage discrete peristaltic micropump, *Sensors and Actuators A: Physical*, 104, 6–10 (2003).
35. D. Tripathi and O Anwar Bég, A study of unsteady physiological magneto-fluid flow and heat transfer through a finite length channel by peristaltic pumping, *Proc. Institution of Mechanical Engineers, Part H: J. Engineering in Medicine*, 226, 631-644 (2012).
36. G. Mao *et al.*, Dielectric elastomer peristaltic pump module with finite deformation, *Smart Mater. Struct.*, 24, 075026 (2015).
37. L. Loumes, Multilayer impedance pump: a bio-inspired valveless pump with medical applications, *PhD Dissertation, California Institute of Technology, Pasadena, USA* (2007).
38. T. Hayat, F.M. Abbasi, M. Al-Yami, S. Monaquel, Slip and Joule heating effects in mixed convection peristaltic transport of nanofluid with Soret and Dufour effects, *J. Mol Liq.*, 194, 93–99 (2014).
39. F.M. Abbasi, T. Hayat, B. Ahmad and G.Q. Chen, Peristaltic motion of non-Newtonian nanofluid in an asymmetric channel, *Z. Nat.* 69A, 451–461 (2014).

40. O. Anwar Bég and D. Tripathi, Mathematical simulation of peristaltic pumping in double-diffusive convection in nanofluids: a nano-bio-engineering model, *Proc. IMechE.- Part N: J. Nanoengineering and Nanosystems*, 225, 99-114 (2012).
  41. K. Maruthi Prasad, N. Subadra, M. A. S. Srinivas, Peristaltic transport of a nanofluid in an inclined tube, *American J. Computational and Applied Mathematics*, 5 117-128 (2015).
  42. C. Dhanapal, J. Kamalakkannan, J. Prakash, M. Kothandapani, Analysis of peristaltic motion of a nanofluid with wall shear stress, microrotation, and thermal radiation effects, *Applied Bionics and Biomechanics*, 2016, 1-15 (2016).
  43. F.M. Abbasi, T. Hayat, B. Ahmad, Peristaltic transport of an aqueous solution of silver nanoparticles with convective heat transfer at the boundaries, *Canadian J. Physics*, 93(10): 1190-1198 (2015).
  44. S. Chakraborty, Augmentation of peristaltic microflows through electro-osmotic mechanisms, *J. Phys. D: Appl. Phys.* **39** 5356 (2006).
  45. D. Tripathi, S. Bhushan and O. Anwar Bég, Transverse magnetic field driven modification in unsteady peristaltic transport with electrical double layer effects, *Colloids and Surfaces A: Physicochem. Engineering Aspects*, 506, 32–39 (2016).
  46. A. Bandopadhyay, D. Tripathi and S. Chakraborty, Electroosmosis-modulated peristaltic transport in microfluidic channels, *Phys. Fluids*. (2016). DOI: 10.1063/1.4947115
  47. M.A. Bosse, P. Arce, Role of Joule heating in dispersive mixing effects in electrophoretic cells: convective-diffusive transport aspects, *Electrophoresis*, 21, 1026–1033 (2000).
  48. N.J. Petersen, R.P. Nikolajsen, K.B. Mogensen and J.P. Kutter, Effect of Joule heating on efficiency and performance for microchip-based and capillary-based electrophoretic separation systems: a closer look, *Electrophoresis*, 25, 253-69 (2004).
  49. A. Sadeghi, M. H. Saidi, H. Veisi, M. Fattahi, Thermally developing electroosmotic flow of power-law fluids in a parallel plate microchannel, *Int. J. Thermal Sciences*, 61, 106-117 (2012).
  50. S. Chakraborty and S. Roy, Thermally developing electroosmotic transport of nanofluids in microchannels, *Microfluid. Nanofluid.*, 4, 501–511 (2008).
-